JOURNAL OF GUIDANCE, CONTROL, AND DYNAMICS
Vol. 19, No. 3, May–June 1996

Experimental Evaluation of an Adaptive Controller for a Wind-Driven Pitch Manipulator

J. C. Magill,* N. M. Komerath,† and J. F. Dorsey‡
Georgia Institute of Technology, Atlanta, Georgia 30332-0150

The problem of control design for wind-driven manipulators is addressed, and results of an experimental controller evaluation are described. Successful control design is essential to the use of the wind-driven manipulator for simulating aircraft maneuvers in a wind tunnel. Several wind-driven manipulator configurations are described. A second-order nonlinear state model for a pitch only manipulator is derived and validated with experimental data. An adaptive feedback linearization algorithm for the pitch manipulator is described. Experimental results are presented to show actual controller performance.

Nomenclature

$\boldsymbol{B}$	= parameter vector
$\hat{\boldsymbol{B}}$	= parameter vector estimate
(c, γ)	= location of center of gravity, polar coordinates
c_w	= control wing chord
$D(\alpha)$	= drag produced by control wing
e	= tracking error, $\Theta_d - \Theta$
e_1	= augmented error used for parameter updates
g_1, g_2	= adaptation gains
J	= inertia of rotating assembly
$\hat{J}$	= inertia estimate
J_{nom}	= nominal inertia
k_d	= error derivative gain
k_e	= error filter parameter
k_p	= error proportional gain
$L(\alpha)$	= lift produced by control wing
l	= length of manipulator arm
$M_a(\Theta, \dot{\Theta}, \phi)$	= aerodynamic pitching moment because of manipulator
$M_{a,1}(\Theta, \dot{\Theta}, \phi)$	= state component of $M_a(\Theta, \dot{\Theta}, \phi)$
$M_{a,2}(\Theta, \dot{\Theta}, \phi)$	= input scaling component of $M_a(\Theta, \dot{\Theta}, \phi)$
$M_g(\Theta)$	= pitching moment because of gravity
$M_m(\Theta, \dot{\Theta})$	= aerodynamic pitching moment because of test model
$N_{\text{arm}}(\Theta, \dot{\Theta})$	= aerodynamic normal force on arm and servo
T	= sampling period
U_∞	= freestream velocity
u_w	= horizontal component of flow velocity in wing reference frame
v_w	= vertical component of flow velocity in wing reference frame
W	= weight of manipulator arm and test model
α	= effective angle of attack of control wing
α_i	= induced angle of attack
β_i	= unknown parameters
$\hat{\beta}_i$	= parameter estimates used in control
Θ	= pitch angle of test model
Θ_d	= desired pitch angle
Λ	= inertia ratio
ξ	= generalized control input
τ_L	= convective time constant for control wing
ϕ	= wing incidence angle (input)
Ψ	= arm attachment angle
ω_c	= filter cutoff frequency

Subscripts

u, k	= unknown and known components of a term

Presented as Paper 94-3657 at the AIAA Guidance, Navigation, and Control Conference, Scottsdale, AZ, Aug. 1–3, 1994; received March 16, 1995; revision received Sept. 11, 1995; accepted for publication Sept. 11, 1995.

*Ph.D. Candidate, School of Electrical and Computer Engineering; Research Assistant, School of Aerospace Engineering; currently Principal Engineer, Physical Sciences, Inc., 20 New England Business Center, Andover, MA 01810. Student Member AIAA.

†Professor, School of Aerospace Engineering. Associate Fellow AIAA.

‡Professor, School of Electrical and Computer Engineering.

Introduction

TO study the complex, unsteady flows over maneuvering aircraft, it is essential to have a means of recreating the maneuvers in a wind tunnel. A wide range of mechanisms have been used for this purpose.[1–4] Forced oscillation devices such as rotary rigs and pitch, roll, or yaw oscillatory drivers are generally limited to motion in one degree of freedom (DOF). Many of these devices use large electrical or hydraulic devices to impart the motion, and periodic motion is generally achieved using cams or cranks to convert rotational motion to sinusoidal motion.

Free-flight and semifree-flight models have also been used in wind tunnels for some types of dynamic testing. These models, however, are limited to the maneuvers that can presently be performed, under strict control, with existing flight control technology. A forced motion rig enables the study of maneuvers that may not presently be possible but are envisioned for future aircraft equipped with more advanced flight controls. Wind-tunnel testing also offers the important advantage that errors can be corrected through repeated refinement of the maneuver during testing, with much less risk and control sophistication than free-flight testing. This makes adaptive control especially attractive for this application.

Some multiple DOF devices, such as the Virginia Polytechnic Institute plunge-pitch-roll manipulator,[5] have been developed to study multiaxis motion. Mechanisms that can move a model in several DOF are necessary for the study of complex maneuvers, especially when exploring the high-α regime where the lateral and longitudinal dynamics are coupled. The design of multiple-DOF manipulators is difficult because either a complex linkage must be designed to move the model with actuators secured in the ground reference frame, or the actuators must be mounted on the moving elements of the manipulator. The latter is the most practical choice for three or more DOF, but it results in large actuators at the base links of the manipulator to move the actuators in the upper links. Massive motors or hydraulic drivers are expensive, typically have low bandwidths, and often result in significant flow interference. Large manipulators may also require facility modification because of the large transient reaction forces borne by the wind tunnel support structure.

The wind-driven dynamic model manipulator (WDM) was developed as a solution to the problem of simulating aircraft maneuvers in the wind tunnel.[6] The WDM relies on kinetic energy in the freestream to induce model motion and thus employs very small actuators. As with some hydraulic devices, and in contrast to

cam-driven oscillation systems, the WDM enables arbitrary maneuvers, limited only by the number of DOF of the manipulator and the maximum achievable rates. The use of wind energy, however, enables development of a much lighter and less intrusive manipulator than is possible with any other drive concept. This is the motivation for the work described in this paper.

The control design problem is broken down into two parts. The first task is to develop and validate a mathematical model that captures the behavior of the wind-driven manipulator. The second task is to design a controller that guarantees stability of the prescribed trajectory in the presence of uncertainty in the mathematical model. Both of those tasks are described in the remainder of this paper. The control design is done for a single-DOF pitch-only manipulator and the results of controller evaluation experiments are presented.

Description of the Manipulator

Figure 1 shows a WDM. A pair of wings are attached at one end of a lever arm. The angle between the wind chord line and the arm can be adjusted with a small servomotor. The other end of the arm is attached to the model mounting block, to which a test model may be attached. The mounting block (and hence the model) pivot on a pitch axle. Lift and drag forces acting on the control wing result in a moment applied to the mounting block and thus cause pitching motion of the model. The control wing pivot point is placed at the quarter chord, and the wing is symmetric, so that the servo need not bear aerodynamic loads and must only produce enough torque to overcome the wing inertia. Thus with very small servo motors, fairly large pitching moments can be produced because all of the necessary energy is taken from the freestream. Because the aerodynamic forces available from the wings increase with the square of the wind velocity, the rates available from the WDM increase with the square of the tunnel speed. Since the real rate required for a given reduced rate increases only linearly with velocity, the WDM is more effective at higher speeds. The major limitations are structural.

By controlling the wing incidence angle, the moment applied to the model can be controlled. With the addition of pitch angle feedback, a controller can be devised that will cause the model to follow a specified pitch trajectory. This can be done without using a perfectly stiff (and massive) manipulator and without prior knowledge of the aerodynamic forces on the model.

Thus far, the authors have built and tested a pitch manipulator and a pitch-yaw manipulator.[7] Some single- and multiple-DOF configurations are shown in Fig. 2. The second DOF (yaw) was achieved by allowing the model to pivot about a vertical axis and installing a set of vertical wings to produce the yawing moment. The equations for the 2-DOF system are more complicated than for the pitch-only WDM because there are interaction terms between the pitch and yaw equations of motion. A 3-DOF roll–pitch–yaw device has the model mounted from the rear, and a differential deflection of wings on opposite sides drives roll.

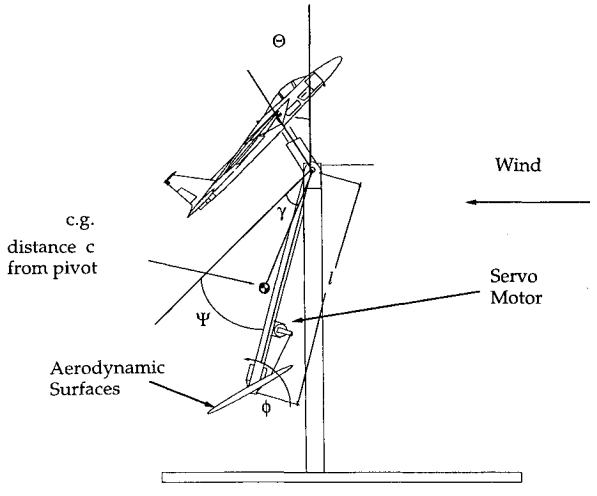

Fig. 1 Wind-driven pitch manipulator with nomenclature.

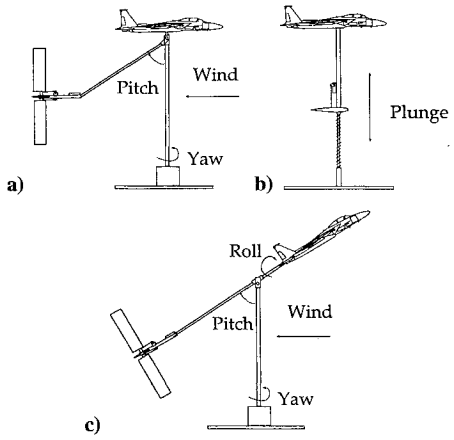

Fig. 2 Possible configurations for wind-driven manipulators: a) pitch/yaw, b) plunge, and c) roll/pitch/yaw.

The WDM exhibits nonlinear dynamics resulting in part from its rotating geometry and in part from the behavior of aerodynamic surfaces. Hence, it is expected that a control design that accounts for the nonlinearities will be needed. The control problem is further complicated by uncertainties in the dynamics because of aerodynamic and inertial differences between the aircraft models being tested. This paper is concerned with developing control laws for a single-DOF pitch manipulator.

Mathematical Model

In this section, the equations of motion for the wind-driven pitch manipulator are derived. Nomenclature is given in Fig. 1. Since there is only one DOF, the dynamics are represented by a torque balance equation,

$$J\ddot{\Theta} = M(\Theta, \dot{\Theta}, \phi) \tag{1}$$

where J is the moment of inertia of the entire pivoting assembly about the axis of motion and ϕ is the angle of incidence of the wing with respect to the arm, measured so that if Θ and ϕ are both zero, the wing chord line is horizontal. $M(\Theta, \dot{\Theta}, \phi)$ is the net moment effected on the manipulator by aerodynamic and gravitational terms. The remainder of the derivation will focus on developing a more detailed expression for this moment.

The net moment may be broken into three components: $M_g(\Theta)$, $M_a(\Theta, \dot{\Theta}, \phi)$, and $M_m(\Theta, \dot{\Theta})$. Since experimental measurement of the test model aerodynamics is a primary purpose for the WDM, the last term will not be written in any greater detail. Instead, it will be treated as an unknown quantity in the control design.

The gravity moment is easily expressed in terms of the c.g. displacements (c, γ) and the weight of the pivoting assembly W:

$$M_g(\Theta) = cW\cos(\Theta + \gamma)$$

The aerodynamic moment $M_a(\Theta, \dot{\Theta}, \phi)$ results from drag and lift acting on the pivot through some moment arms that vary with the instantaneous pitch angle Θ. Most of this moment is caused by the control wing, although the arm and other hardware also contribute. It is important to develop a detailed expression for this term because it contains the control input.

It will be assumed that the unsteady aerodynamics of the control wing are fast. The time constant for the decay of the unsteady lift is approximated by $\tau_L = c_w/U_\infty$. With a wing chord of 11.4 cm and a freestream velocity of 17 m/s, the time constant of the unsteady lift is 0.0067 s, about 10 times faster than the dynamics of the rotating assembly. Thus, a quasisteady description of the wing aerodynamics will be used so that the lift L and drag D on the wing are functions of its effective angle of attack α.

Experimental data are available relating lift and drag of the wing to its angle of attack. The task remaining, then, is to find an expression for the effective angle of attack by identifying the velocity vector of the wing quarter-chord in the wing reference frame. This expression consists of the geometric angle between the wing and the freestream

plus a term resulting from the placement of the wing at the end of the rapidly pivoting arm. The streamwise component of the velocity vector is

$$u_w = U_\infty + l\sin(\Theta + \Psi)\dot{\Theta}$$

The second term will generally be less than 5% of the first. The vertical component of the velocity is

$$v_w = l\cos(\Theta + \Psi)\dot{\Theta}$$

The induced angle of attack can be expressed as

$$\alpha_i = \tan^{-1}\left(\frac{l\cos(\Theta + \Psi)\dot{\Theta}}{U_\infty + l\sin(\Theta + \Psi)\dot{\Theta}}\right)$$

so that $\alpha = \alpha_i + \Theta + \phi$. An expression for the aerodynamic moment can now be written as

$$M_a(\Theta, \dot{\Theta}, \phi) = -l[L(\alpha)\cos(\Theta + \Psi + \alpha_i) + D(\alpha)\sin(\Theta + \Psi + \alpha_i)] - (l/2)N_{\text{arm}}(\Theta, \dot{\Theta})$$

The arguments of the sin and cos functions that determine the moment arms both contain the term α_i. This was done because the lift and drag forces are resolved normal and parallel to the relative velocity vector. Note also that a term $N_{\text{arm}}(\Theta, \dot{\Theta})$ has been added to account for aerodynamic forces on the arm.

For the purpose of control design, lift is assumed to be a linear function of the angle of attack. There is nothing to be gained by pushing the control wings into stall because the full range of force from the wing is available in the unstalled portion of the lift curve.

Collecting equations, the complete model is

$$J\ddot{\Theta} = Wc\cos(\Theta + \gamma) - l[L(\alpha)\cos(\Theta + \Psi + \alpha_i) + D(\alpha)\sin(\Theta + \Psi + \alpha_i)] - (l/2)N_{\text{arm}}(\Theta, \dot{\Theta}) + M_m(\Theta, \dot{\Theta}) \quad (2)$$

which is a second-order nonlinear system.

Model Validation

To validate the nonlinear model, a mathematical model output and the actual output of the experimental system were compared for the same input. To compare the two, an input containing several frequencies was applied to the servomotor on the pitch manipulator with the tunnel operating at a speed of 17 m/s. No aircraft model was attached, so that $M_m(\Theta, \dot{\Theta}) = 0$. A position encoder on the wing axle was used to measure ϕ, the input variable in Eq. (2), as a function of time. The data acquisition system sampled the pitch encoder and the wing encoder at 61 Hz to capture the time histories of Θ and ϕ. The samples of ϕ were then used as the input for a MATLAB/SIMULINK™ simulation of Eq. (2) using the system geometry and measured control wing lift and drag data to compute the model parameters. The Θ values measured during the actual experiment were compared to those generated by the simulator to test model validity. The parameters used in the simulation are shown in Table 1. Figure 3 shows the comparison of the two signals for an excitation of moderate amplitude. The simulation output had a higher amplitude than that of the experiment, and the root mean square error was 2.6 deg. The simulation included no terms to account for drag on the arm or servo. In an effort to match a model to the data, the damping was increased by different amounts until matching was achieved. The increase was accomplished by scaling the induced angle of attack. Though the wing itself is not the sole source of unmodeled damping, an easy way to increase the damping is to scale up α_i. When the damping in the simulation was increased by 50% (Fig. 4), the experiment matched the simulation nicely, with an rms error of only 0.9 deg. When the control wing excitation amplitude was increased (Fig. 5) the matching deteriorated slightly, and the rms error increased to 2.3 deg. This indicates that higher order damping terms may be at work. Though these results do not prove conclusively that the model Eq. (2) is correct, they provide some confidence that the model order has been chosen correctly and that the calculated parameters are close to the actual system parameters.

In the latter three experiments, an offset of 0.47 deg was added to the simulation to account of a constant discrepancy between the two signals. It was necessary because incremental encoders were used, and there is some uncertainty (less than 0.5 deg) in the measurement of the absolute angle, which is accomplished with a hand-held inclinometer.

Table 1 Values of parameters used in simulations

Parameter	Value
Ψ	30 deg
γ	30 deg
c	31.5 cm
W	0.607 kg
J	0.100 kg m^2
l	45.7 cm
S	0.031 m^2
q_∞	174.3 N/m^2
U_∞	17.1 m/s
$\partial L/\partial\alpha$	3.84 q_∞S N/rad
D	q_∞ S(2.1 α^2 + 0.063) N

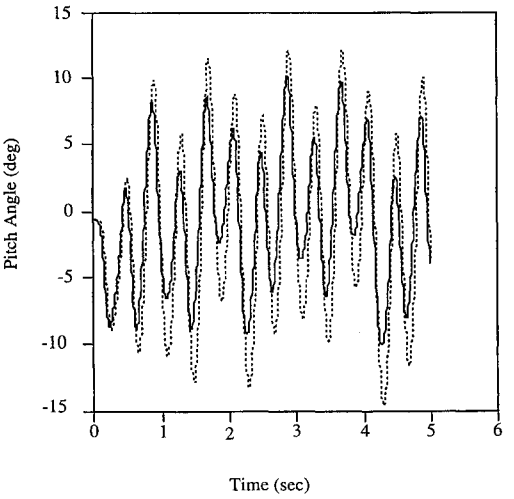

Fig. 3 Comparison of simulation and experiment for validation of a nonlinear mathematical model of the wind-driven pitch manipulator; angle measurement error ±0.088 deg: ——, experiment and - - - -, simulation.

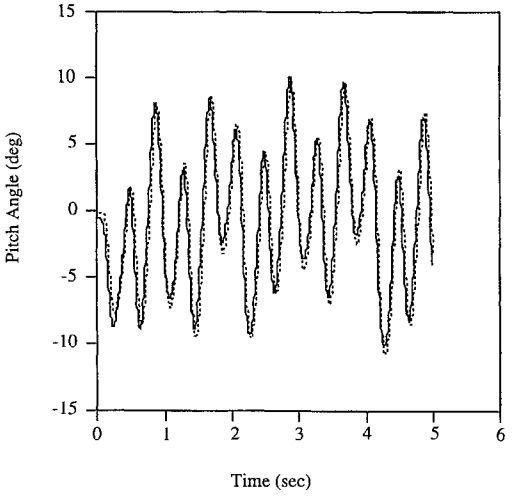

Fig. 4 Comparison of simulation and experiment for validation of a nonlinear mathematical model of the wind-driven pitch manipulator; simulation had 50% damping increase and 0.47-deg output offset; angle measurement error ±0.088 deg: ——, experiment and - - - -, simulation.

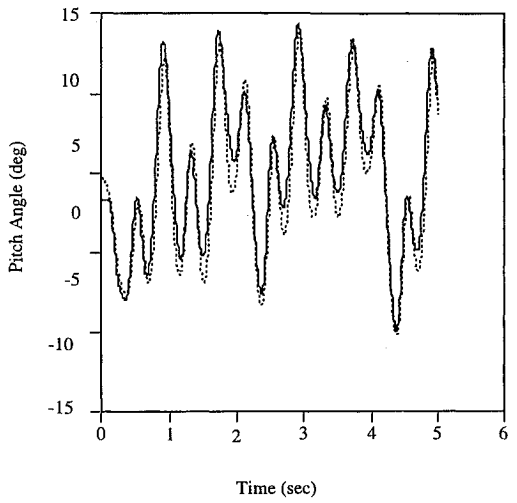

Fig. 5 Large-amplitude comparison of simulation and experiment for validation of a nonlinear mathematical model for the pitch manipulator; simulation had a 50% damping increase and 0.47-deg output offset; angle measurement error ±0.088 deg: ——, experiment and - - - -, simulation.

Adaptive Controller Design

Controller Requirements

The controller must provide stable tracking of prescribed trajectories. The magnitude of tolerable error depends on the specific application. Most often, the trajectory will be available to the controller before tracking begins, and desired position, rate, and acceleration will be provided.

The aerodynamic forces and moments that would act on an aircraft model during testing will generally be unknown since the purpose of the test is often to measure these. Hence, the closed-loop tracking properties of the system must be robust to fairly large uncertainties. It will usually be possible to parameterize the uncertainties or bound them with simple bounding functions.

State Equation Modification

In this section, an approximation will be given that transforms the mathematical model into a more manageable form, and the model uncertainty is parameterized. The control and adaptation laws will be given here with some explanation, but details of their derivation and stability are omitted, as this paper addresses only the experimental results. A complete development and stability proof are given in Ref. 8.

The mathematical model for the manipulator can be simplified with an approximation that leaves the input decoupled from the rest of the pitching moments. Since it is only necessary to operate the control wing on the unstalled portion of the lift curve, lift is approximately a linear function of the effective angle of attack. The drag can be approximated by a linear expansion in ϕ,

$$D(\alpha_i + \Theta + \phi) \cong D(\alpha_i + \Theta) + \phi \frac{\partial D}{\partial \alpha}(\alpha_i + \Theta)$$

The aerodynamic moment resulting from the manipulator itself can be rewritten

$$M_a(\Theta, \dot{\Theta}, \phi) = -l\left\{\left(\frac{\partial L}{\partial \alpha}\right)(\Theta + \alpha_i + \phi)\cos(\Theta + \Psi + \alpha_i) + \left[D(\Theta + \alpha_i) + \phi \frac{\partial D}{\partial \alpha}(\Theta + \alpha_i)\right]\sin(\Theta + \Psi + \alpha_i)\right\} - \frac{l}{2} N_{\text{arm}}(\Theta, \dot{\Theta})$$

This can, in turn, be separated into a state function

$$M_{a,1}(\Theta, \dot{\Theta}) = -l\left[\left(\frac{\partial L}{\partial \alpha}\right)(\Theta + \alpha_i)\cos(\Theta + \Psi + \alpha_i) + D(\Theta + \alpha_i)\sin(\Theta + \Psi + \alpha_i)\right] - \frac{l}{2} N_{\text{arm}}(\Theta, \dot{\Theta})$$

and an input sensitivity

$$M_{a,2}(\Theta, \dot{\Theta}) = -l\left[\left(\frac{\partial L}{\partial \alpha}\right)\cos(\Theta + \Psi + \alpha_i) + \sin(\Theta + \Psi + \alpha_i)\frac{\partial D}{\partial \alpha}(\Theta + \alpha_i)\right]$$

so that $M_a(\Theta, \dot{\Theta}) = M_{a,1}(\Theta, \dot{\Theta}) + M_{a,2}(\Theta, \dot{\Theta})\phi$.

Fortunately, $M_{a,2}(\Theta, \dot{\Theta})$ is always nonzero for the desired range of motion, so that a new generalized input ξ can be defined with $\xi = M_{a,2}(\Theta, \dot{\Theta})\phi$. Then, if ξ is used as the control input, the actual wing angle that must be used is

$$\phi = \frac{\xi}{M_{a,2}(\Theta, \dot{\Theta})}$$

Now, the equation of motion for the manipulator and test model combination can be written as

$$J\ddot{\Theta} - M_{a,1}(\Theta, \dot{\Theta}) - M_m(\Theta, \dot{\Theta}) - M_g(\Theta) = \xi$$

The form of this equation mimics the common form for a robot manipulator[9] with J being the inertia matrix and $-M_{a,1}(\Theta, \dot{\Theta}) - M_m(\Theta, \dot{\Theta}) - M_g(\Theta)$ paralleling the Coriolis terms. Hence, an adaptive controller designed for robot manipulators[8] will be used.

Before designing the controller it is necessary to parameterize the uncertainty in the model. The input sensitivity $M_{a,2}(\Theta, \dot{\Theta})$ is known because wing measurements are easily made on a static balance. The contribution of the wing itself to $M_{a,1}(\Theta, \dot{\Theta})$ is known, but the component of this function due to drag on the arm and servo are not known. Hence, $M_{a,1}(\Theta, \dot{\Theta})$ is split into two components: a known element

$$M_{a,1,k}(\Theta, \dot{\Theta}) = -l\left[\left(\frac{\partial L}{\partial \alpha}\right)(\Theta + \alpha_i)\cos(\Theta + \Psi + \alpha_i) + D(\Theta + \alpha_i)\sin(\Theta + \Psi + \alpha_i)\right]$$

and an unknown element $M_{a,1,u}(\Theta, \dot{\Theta})$. The gravitational moment can also be split into known and unknown parts, and the model moment is completely unknown.

It is necessary to assume some parametric form for the unknown pitching moment. For wind-tunnel tests of aerodynamic models, this will generally be based on experience with a particular class of airframes. With some knowledge of the types of moments that are expected, it is often possible to choose the functions to give good approximations for a family of anticipated moment functions. For example, moments produced by a tail are expected to be almost linear for small angles of attack and concave downward at higher angles, and so a parabolic or cubic function might be chosen to represent its contribution. A wing moment may also be expected to be a polynomial function of the angle of attack. If the wing and tail are the dominant contributions to the moment, then the highest order of the two polynomials would be used as the parametric model.

It is beneficial also to minimize the number of undetermined parameters to simplify computation by the controller. A few trials with any graphing software can be used to determine whether two potential basis functions or combinations of functions are nearly proportional to one another over the range of operation. If so, the simpler of the two may be used and the other discarded.

In the experiments described herein it was assumed that the sum of the unknown aerodynamic and gravitational moments had the form

$$M_{a,1,u}(\Theta, \dot{\Theta}) + M_m(\Theta, \dot{\Theta}) + M_{g,u}(\Theta) = \beta_0 \cos(\theta + \Psi) - \beta_1 \Theta \cos(\Theta) - \beta_2(\dot{\Theta}/U_\infty)\cos\Theta + \beta_3 \Theta|\Theta|\cos(\Theta)$$

where the β are unknown coefficients. The inertia of the manipulator plus model combination was also treated as an unknown. Though

this parameterization is not exact, it provides versatility. If there is multiplicative uncertainty in $M_{a,2}(\Theta, \dot{\Theta})$, it can be accommodated approximately by adjusting the unknown parameters and inertia until good tracking is achieved. The term $\beta_0 \cos(\Theta + \Psi)$ is used to capture the gravitational moments, but Ψ and γ are not exactly equal. The manipulator mass dominates that of the model, however, so that Ψ and γ are close to one another, and the error can be nearly recovered by the $\Theta \cos \Theta$ term. The second and third terms are low-order stiffness and damping components. The last term is a higher order stiffness term that is important over highly nonlinear aerodynamic regions, such as the poststall regime. The choice of these functions is the designer's prerogative, and the ones used here are not necessarily the best choice, but will be shown to yield good performance.

Control and Adaptation Laws

The adaptive controller described here is an output-error indirect scheme, and is similar to one given in Sastry and Bodson (Sec. 7.3.3),[8] where the reader may find a complete treatment of the material in this section. It consists of two components: an identifier and a controller. If all of the plant parameters are known, the control law

$$\xi = [M_g(\Theta) + M_a(\Theta, \dot{\Theta}) + M_m(\Theta, \dot{\Theta})] + J(k_d\dot{e} + k_p e + \ddot{\Theta}_d) \quad (3)$$

would be used, where the tracking error is defined as the difference between the desired and actual trajectory $e = \Theta_d - \Theta$, and the error derivative as $\dot{e} = \dot{\Theta}_d - \dot{\Theta}$. Since the right-hand side (RHS) of Eq. (3) is not known exactly, a best guess of the ideal control law is used. This constitutes the controller element. In parallel with the controller, the identifier is continuously improving the estimates of the WDM parameters based on input and state measurements. These estimates are made available to the controller. As time passes, knowledge on the terms on the RHS of Eq. (3) is improved, and tracking performance improves as a consequence.

Employing the estimated quantities, denoted by an overbar, the feedback law is

$$\xi = \bar{J}\ddot{\Theta}_d + k_p e + k_d \dot{e} - M_{a,1,k}(\Theta, \dot{\Theta}) - M_{g,k}(\Theta)$$
$$- \bar{\beta}_0 \cos(\theta + \Psi) + \bar{\beta}_1 \Theta \cos(\Theta) + \bar{\beta}_2 \left(\frac{\dot{\Theta}}{U_\infty}\right) \cos \Theta$$
$$- \bar{\beta}_3 \Theta |\Theta| \cos(\Theta)$$

where the best guess of the nonlinearities are fed back to cancel those of the system, proportional-derivative terms $k_p e$ and $k_d \dot{e}$ are used to counter disturbances and remove initial error, and the desired acceleration $\ddot{\Theta}$ is fed forward.

Note that two derivatives of the desired angle are required. These are easily obtained with proper trajectory planning since any real trajectory will have bounded rates and accelerations. To compose the adaptation law, define the vectors

$$\bar{\boldsymbol{B}} = [\bar{\beta}_0 \quad \bar{\beta}_1 \quad \bar{\beta}_2 \quad \bar{\beta}_3]^T$$

$$\boldsymbol{F} = \frac{1}{J}\left[\cos(\Theta + \Psi) \quad -\Theta \cos(\Theta) \quad -\frac{\dot{\Theta}}{V} \cos \Theta \quad \Theta|\Theta| \cos(\Theta)\right]^T$$

and the inertia ratio Λ such that

$$\bar{J} = \Lambda J_{\text{nom}}$$

where J_{nom} is a nominal inertia value chosen by the designer. This is done so that the adapting parameter Λ will be of the same order of magnitude as the parameters in $\bar{\boldsymbol{B}}$. An augmented error will be used in the parameter update laws. The new error signal is

$$e_1 = \dot{e} + k_e e$$

The gradient type adaptation law is

$$\dot{\bar{\boldsymbol{B}}} = g_1 \boldsymbol{F} e_1 \qquad \text{and} \qquad \dot{\Lambda} = -g_2 (1/\bar{J}) \ddot{\Theta} e_1$$

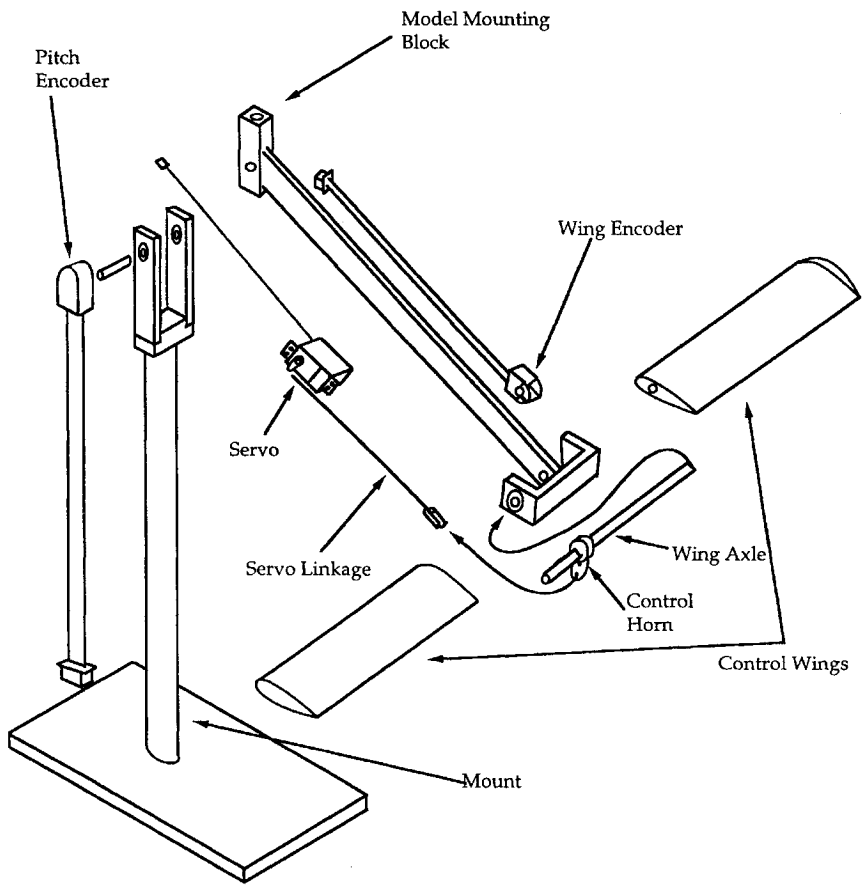

Fig. 6 Details of construction of wind-driven pitch manipulator.

where g_1 and g_2 are positive scalar adaptation gains. A sufficient condition for stable tracking is that the transfer function

$$\frac{(s+k_e)}{(s^2+k_d s+k_p)}$$

be strictly positive real.

Experimental Setup and Controller Implementation

The tracking control experiments were performed on a pitch manipulator constructed as shown in Fig. 6. The control wings had NACA 0012 airfoils with a 10-cm chord and a 30.5-cm span. The arm from the wings to the mounting block was 45 cm long, and the stand was 61 cm high. It is capable of angles of attack up to 45 deg and has exhibited pitch rates in excess of 180 deg/s with freestream velocity of 17 m/s.

The School of Aerospace Engineering's low-turbulence wind tunnel was used for the experiments. This tunnel is an open return type with a 1.2 × 1.2 m test section and an upstream blower.

An Intel 80386-based personal computer was used as the control computer. Angle feedback was taken from an optical encoder with quadrature output mounted on the manipulator pitch axle. The encoder resolution was 2048 counts/rev, giving an error of ±0.088 deg. An encoder interface board was used to track the quadrature signals. The servomotor was a model airplane servo commanded by the control computer through a pulse modulator. Figure 7 shows the control system block diagram.

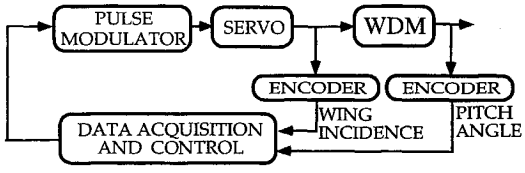

Fig. 7 Data acquisition and control system block diagram for adaptive control experiments.

Continuous time integration of parameter updates was approximated by a first-order estimate:

$$x_{n+1} = x_n + \frac{\mathrm{d}x}{\mathrm{d}t_n} T$$

The sampling period T was 0.0164 s (sampling rate = 61.03 Hz). The controller required estimation schemes for extracting velocity and acceleration data from discrete position measurements. The velocity was estimated by taking a backward difference of the position data, and then low-pass filtering the result.[10] The filter used was a first-order filter with a 14.3-Hz cutoff. The collection of estimation equations with frequency in hertz was

$$\dot{\Theta}_n = f\dot{\Theta}_{n-1} + (1-f)[(1/4T)(\Theta_n - \Theta_{n-4})]$$

$$f = e^{-2\pi\omega_c T} \qquad \omega_c = 14.3$$

The acceleration was, in turn, estimated from the position using a first-order backward difference and a filter

$$\ddot{\Theta}_n = f\ddot{\Theta}_{n-1} + (1-f)[(1/T)(\dot{\Theta}_n - \dot{\Theta}_{n-1})]$$

$$f = e^{-2\pi\omega_c T} \qquad \omega_c = 14.3$$

This is similar to the method given in Hsu et al.,[11] where the acceleration measurement is replaced by a filtered version of the velocity.

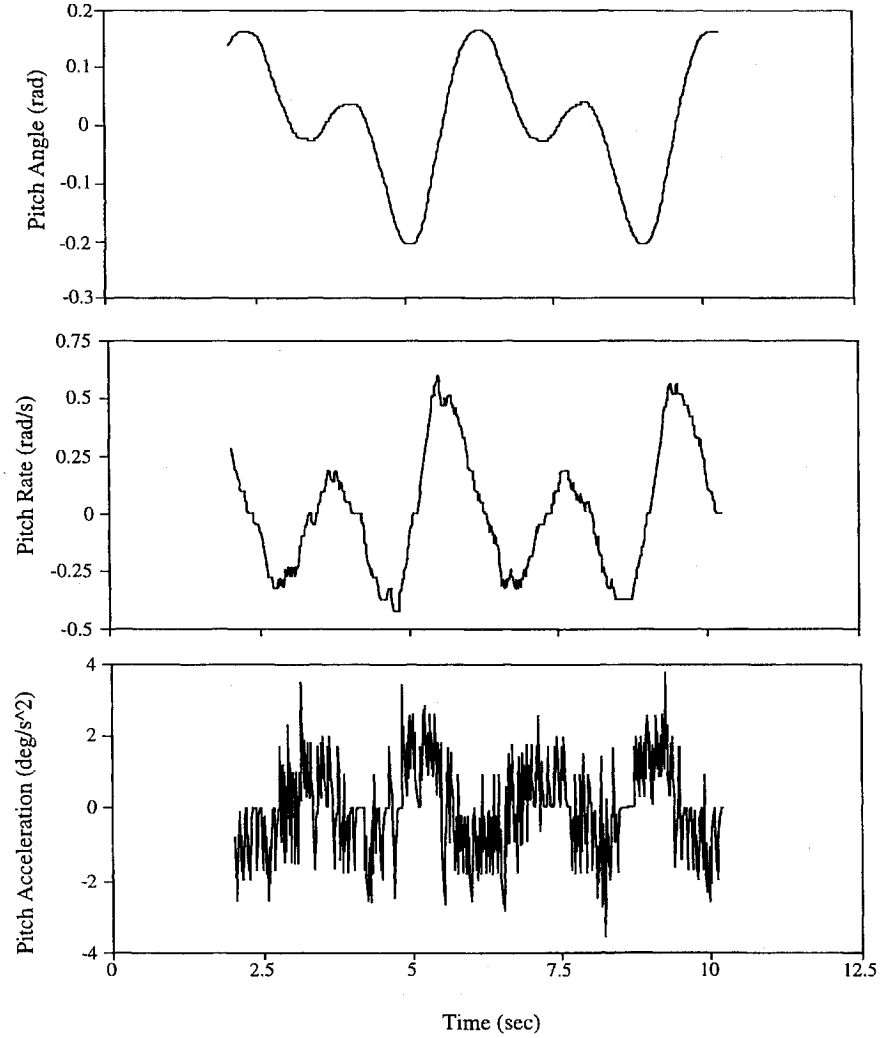

Fig. 8 Position measurements, velocity, and acceleration estimates during a control experiment.

Table 2 Values of known terms for control law

Parameter	Value
Ψ	30 deg
γ	30 deg
c	26.7 cm
W	0.607 kg
J_{nom}	0.109 kg m^2
l	45.7 cm
S	0.031 m^2
q_∞	201.3 N/m^2
U_∞	18.5 m/s
$\partial L/\partial\alpha$	4.4 $q_\infty S$ N/rad
D	$q_\infty S(5.25\alpha^2 - 0.35\alpha + 0.063)N$

Figure 8 shows a set of position, velocity, and acceleration signals. The velocity is not very noisy, but the acceleration estimates contain substantial noise. The low-pass characteristics of the plant reject propagation of the noise to the plant output, so good tracking is still possible even with noisy acceleration data.

The controller gains for these experiments were chosen empirically to give good steady-state performance. However, they remained the same for all of the experiments. Indeed, an adaptive controller would not be very useful if it required tuning by the operator each time a new model or new trajectory was used. In these experiments, $k_p = 180$, $k_d = 8$, and $k_e = 8$. Other parameters used to describe the known elements of the feedback law are given in Table 2.

The adaptation gains g_1 and g_2 are chosen to yield quick adaptation, but if they are too large, the parameter estimates may oscillate wildly during the initial phases of adaptation. A couple of trials was sufficient to show that a value of $g_1 = 0.08$ yielded good performance when the inertia was known and no estimate of J was used ($g_2 = 0$). However, $g_1 = 0.08$ was too large once inertia estimates were added, and the controller produced unwanted oscillations. For the experiments involving inertia estimates, adaptation gains of $g_1 = 0.008$ and $g_2 = 0.001$ were used. The retarded adaptation of the inertia relative to the other parameters is necessary in part because of the large noise content in the acceleration estimates.

To prevent bursting of the parameter estimates, i.e., sudden large perturbations in the estimates that decay rapidly, a deadband was applied to the error. In these experiments, the deadband prevented changes in the parameter estimates when the error was less than 1.4 deg or five encoder counts.

Experimental Results

To evaluate the performance of the adaptive controller, experiments were performed with two different aircraft models. One model was a delta wing mounted on the end of a rod with a 30-deg incidence angle (Fig. 9a). The second aircraft was a 1/32-scale F-18 model filled with a heavy foam (Fig. 9b). A maneuver trajectory consisting of a constant initial angle followed by a sum of two sinusoids was prescribed for each model, and the ability of the controller to track the prescribed time history was evaluated. The maneuver lasted 16.7 s and was repeated as the controller was allowed to adapt. The tunnel velocity was 18.4 m/s for all of the experiments.

The first model was fairly light but was aerodynamically very large, accounting for about 25% of the aerodynamic pitching moment. The F-18, although not very large aerodynamically, had an inertia equal to about one-half that of the manipulator itself and, thus, constituted a large uncertainty.

First, the delta wing model was mounted on the manipulator. No adaptation was permitted initially ($g_1 = g_2 = 0$). Figure 10 reveals that this controller resulted in poor tracking of the prescribed trajectory, with both offset and amplitude errors. Then the experiment was repeated with the adaptation turned on (Fig. 11). Immediate improvement is obvious. The tracking can be seen to improve until a steady state was reached after about 2 min (Fig. 12). The experiment was performed again using a different maneuver prescription (Fig. 13). The steady-state tracking is excellent. Some deficiency is noted in Fig. 14, where the prescribed maneuver is faster than

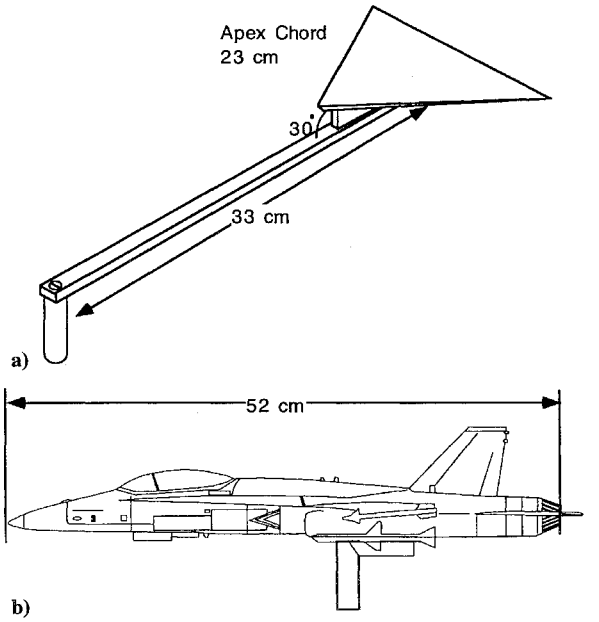

Fig. 9 Models used in tracking control experiments: a) delta wing and b) F-18.

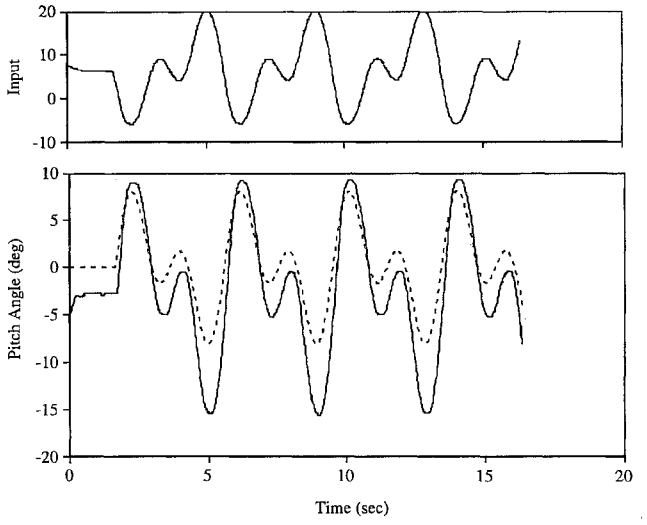

Fig. 10 Nominal linearizing controller performance on pitch manipulator with delta wing model; angle measurement error ±0.088 deg: ——, actual and - - - -, command.

in Fig. 12 and with larger amplitude than Fig. 13. This error can be attributed in part to the neglect of the unsteady aerodynamics of the control wing in deriving the equations of motion. In the delta wing model experiments, no inertia estimate adaptation was used ($g_2 = 0$). Since the model was light in comparison to the manipulator arm, the inertia was assumed known.

Likewise, the steady-state tracking error in the F-18 experiments was small (Fig. 15). In the F-18 experiments, an inertia estimate was used. In fact, the steady-state estimate was 50% higher than for the manipulator alone. Without the inertia estimate, the F-18 tracking performance was hampered significantly.

Whether the parameter estimates converged to their actual physical values was not evaluated. This algorithm only guarantees, in general, that the parameters will converge to some set of values that will cause the tracking error to decay to zero. A requirement on input richness is necessary to guarantee convergence to actual physical values if such a unique set of values does exist. Since good tracking is all that was needed, the values to which the estimates converged were not important.

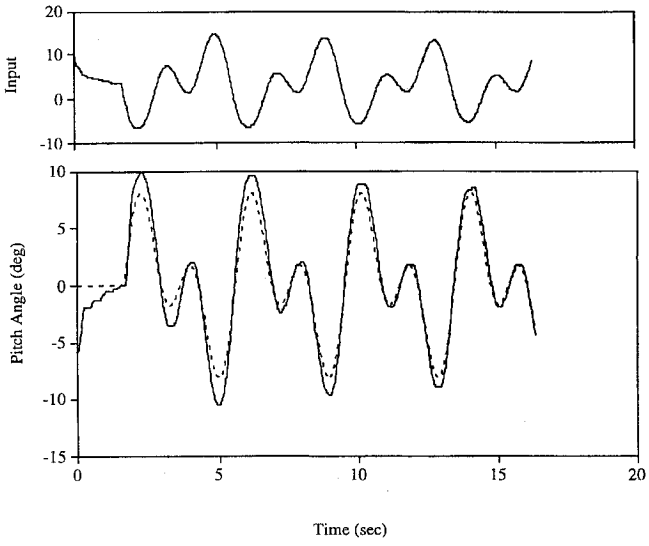

Fig. 11 Adaptive controller performance on pitch manipulator with delta wing just after controller is switched on; angle measurement error ±0.088 deg: ——, actual and - - - -, command.

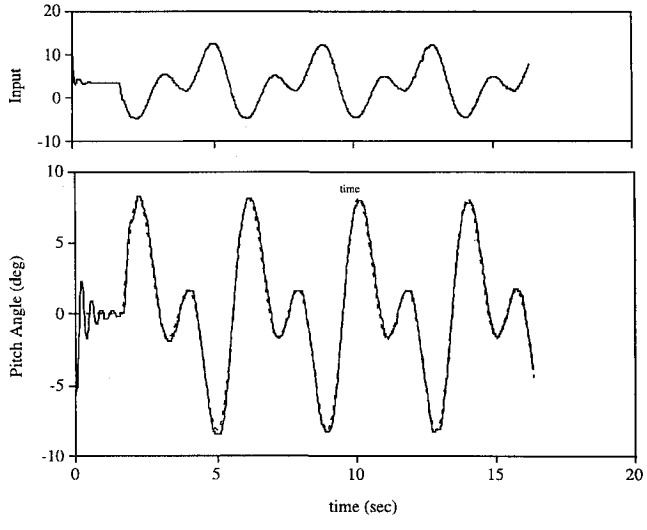

Fig. 12 Steady-state adaptive controller performance on pitch manipulator with delta wing; angle measurement error ±0.088 deg: - - - -, command and ——, actual.

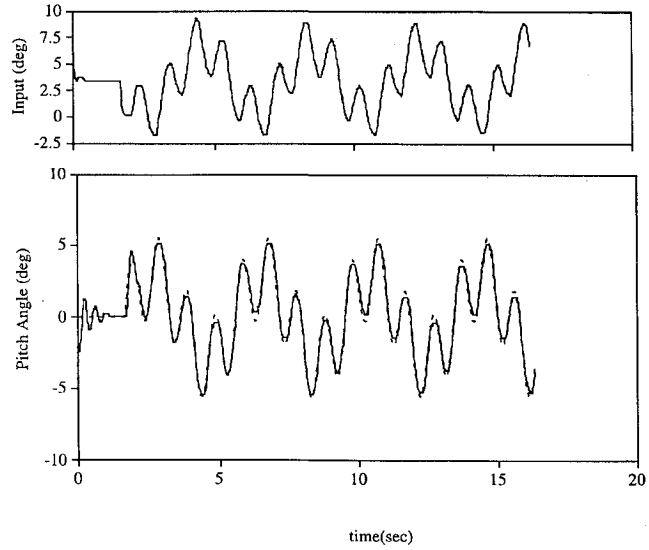

Fig. 13 Steady-state adaptive controller performance on pitch manipulator with delta wing during high-rate maneuver; angle measurement error ±0.088 deg: - - - -, command and ——, actual.

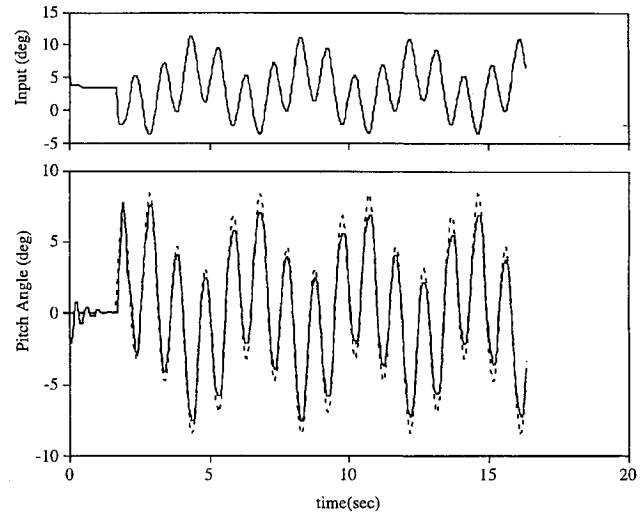

Fig. 14 Steady-state adaptive controller performance on pitch manipulator with delta wing during large-amplitude high-rate maneuver; angle measurement error ±0.088 deg: - - - -, command and ——, actual.

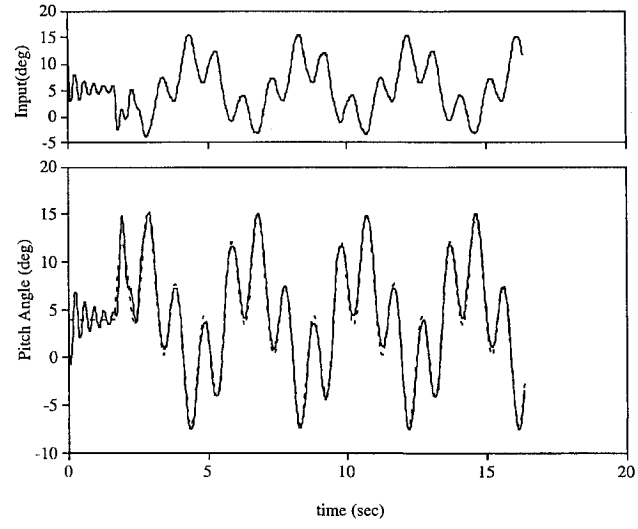

Fig. 15 Steady-state adaptive controller performance on pitch manipulator with F-18 model; angle measurement error ±0.088 deg: - - - -, command and ——, actual.

Conclusions

1) A second-order nonlinear model was derived for a single-DOF wind-driven pitch manipulator. A comparison between the experiment and a numerical simulation of the mathematical model was used to evaluate the model. The outputs matched in phase and differed slightly in amplitude.

2) The mathematical model was simplified, making control design easier. The aerodynamics of the control wing were decoupled from the remainder of the aerodynamic moments.

3) An adaptive nonlinear controller provided good tracking control for a single-DOF wind-driven manipulator in spite of large uncertainties in aerodynamics and inertia of the test models. The same controller was evaluated experimentally with two different test specimens, and the error in tracking a trajectory consisting of two sinusoids decayed in a short time.

These results make it possible to use the WDM for dynamic wind-tunnel experiments. It will now be necessary to extend these results to a multiple-DOF manipulators.

Acknowledgments

This work was supported under U.S. Air Force Office of Scientific Research Grant F49620-93-1-0036 and an associated Augmentation Grant. The Technical Monitors are Maj. Daniel Fant and Len Sakell. The authors gratefully acknowledge the assistance provided by other

members of the Experimental Aerodynamics Group at the School of Aerospace Engineering and valuable discussions with David Taylor in the School of Electrical Engineering.

References

[1]Anon., "Rotary Balance Testing for Aircraft Dynamics," Rept. of the Fluid Dynamics Panel Working Group 11, AGARD-AR-265, Dec. 1990.

[2]Hanff, E. S., "Direct Forced-Oscillation Techniques for the Determination of Stability Derivatives in the Wind Tunnel," *Dynamic Stability Parameters*, AGARD-LS-114, May 1981, pp. 4-1–4-22.

[3]Orlik-Ruckemann, K. J., "Review of Techniques for Identification of Aircraft Stability Parameters in the Wind Tunnel," *Dynamic Stability Parameters*, AGARD-LS-114, May 1981, pp. 3-1–3-28.

[4]Orlik-Ruckemann, K. J., Hanff, E. S., and Anstey, C. R., "Wind Tunnel Apparatus for Translational Oscillation Experiments," AIAA Paper 80-0046, Jan. 1980.

[5]Ahn, S., Choi, K.-Y., and Simpson, R. L., "Design and Development of a Dynamic Plunge-Pitch-Roll Model Mount," AIAA Paper 89-0048, Jan. 1989.

[6]Magill, J. C., and Komerath, N. M., "A Wind-Driven Dynamic Manipulator for Wind Tunnels," *Experimental Techniques*, Vol. 19, No. 1, 1995; U.S. Patent 5,345,818.

[7]Magill, J. C., Darden, L. A., and Komerath, N. M., "Visualization of Rate Dependent Vortex Phenomena During Wind Tunnel Simulation of Aircraft Maneuvers," AIAA Paper 94-0669, Jan. 1994.

[8]Sastry, S., and Bodson, M., *Adaptive Control: Stability, Convergence, and Robustness*, Prentice–Hall, Englewood Cliffs, NJ, 1989, Chap. 8.

[9]Craig, J. J., *Introduction to Robotics: Mechanics and Control*, Addison–Wesley, Reading, MA, 1989, pp. 187–216.

[10]Oppenheim, A., and Schaffer, R., *Discrete Time Signal Processing*, Prentice–Hall, Englewood Cliffs, NJ, 1989, pp. 403–488.

[11]Hsu, P., Bodson, M., Sastry, S., and Paden, B., "Adaptive Identification and Control of Manipulators Without Using Joint Accelerations," *Proceedings of the IEEE Conference on Robotics and Automation* (Raleigh, NC), Inst. of Electrical and Electronics Engineers, 1987, pp. 1210–1215.